Electronic Supplementary Material (ESI) for Journal of Materials Chemistry C.
This journal is © The Royal Society of Chemistry 2014

Electronic Supplementary Information

Highly energy-efficient and air-stable organic transistors by an ultrathin hybrid dielectric with large internal voltage generation

Yu-Wu Wang,[a] *Guan-Yi Tseng,*[a] *Liang-Yun Chiu,*[b] *Bo-Ren Lin,*[b] *Yu-Yang Lin,*[a] *Tsu-Wei Haung,*[a] *Wei-Yang Chou,*[b] *Lance Horng*[c] *and Horng-Long Cheng*[b,*]

[a] Institute of Photonics, National ChangHua University of Education, Changhua 500, Taiwan

[b] Department of Photonics, Advanced Optoelectronic Technology Center, National Cheng Kung University, Tainan 701, Taiwan

[c] Department of Physics, National ChangHua University of Education, Changhua 500, Taiwan

* To whom correspondence should be addressed: e-mail: shlcheng@mail.ncku.edu.tw

Content

1. XPS results

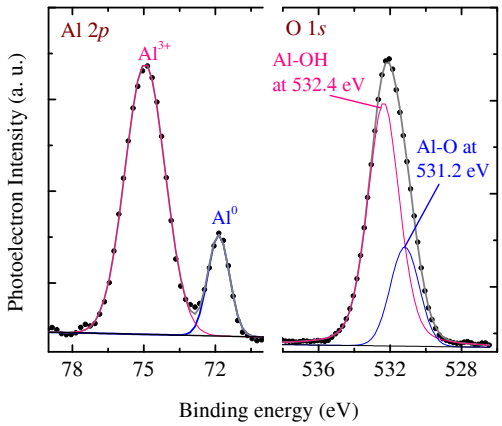

Fig. S1 Normalized Al 2*p* and O 1*s* XPS peaks of ~ 4 nm-thick aluminum oxide films made by oxygen plasma treatment on Al metal. There are two peaks of Al 2*p*. One weaker peak at 71.9 eV indicates metallic Al and the other main peak at 74.9 eV is peculiar to fully oxidized Al.[s1] The O1s peak fit shows two peaks at 531.2 and 532.4 eV. The first peak is as attribute to oxygen in the Al-O-Al bonds, and the second to the Al-O-H bonds.[s1] The data confirmed the formation of the AlO_x nanolayer on Al metal. (Note: XPS were recorded on an ULVAC-PHI PHI 5000 VersaProbe X-ray photoelectron spectrometer.)

2. Leakage current and capacitance properties of the dielectrics

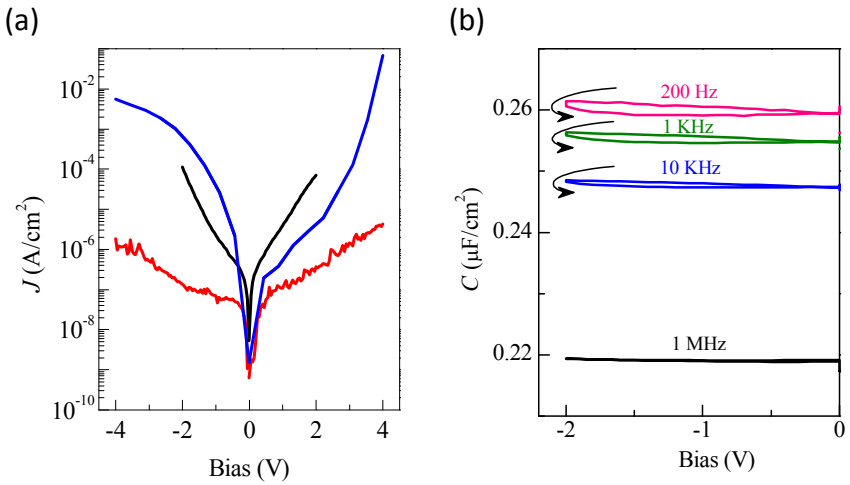

Fig. S2 (a) Leakage current density (*J*) versus applied bias of MIM diodes with different insulators: (black line) AlOx; (red line) CSDE dielectric; (blue line) crosslink-PVP (PVP:PMF of 1:4)/AlOx. (b) Capacitance (*C*) versus applied bias of MIM diodes with the CSDE dielectrics operating at various frequencies.

3. In-situ Raman scattering studies of the interfacial species

Detecting the formation of interfacial molecules between AlO_x-OH and crosslink-PVP is possible by using in-situ Raman spectroscopy combined with quantum chemical calculations. We focused on the Raman spectral regions between 320–420 cm^{-1} and 900–1000 cm^{-1}, as shown in Fig. S3. During the application of a negative voltage on the Al electrode of the CSDE dielectrics sample, we could detect two considerable Raman bands centered at 393 (381) and 950 (938) cm^{-1} using a 532 nm (633 nm) excitation line (traces a and b of Fig. S3). However, the signals could not be detected with no external V_G (trace c, at the moment interfacial molecules at the neutral state) and with a positive V_G (data not shown, at the moment interfacial molecules at the anion state). The two bands cannot also be detected in the AlO_x nanolayer, either without (trace d) or with (trace e) applied voltage on an Al electrode. For the interfacial molecules at the neutral and anion states, theoretical calculations reveal very weak Raman activity (traces g and h, smaller than 80 $Å^4$/amu in the two regions) as compared with that of the cation state (trace f, higher than 10^3 and 10^4 $Å^4$/amu within 320–420 and 900–1000 cm^{-1}, respectively). According to theoretical calculations of the interfacial species at a cation state, the two bands could be assigned to the vibrations involved in the Al-O-CH_2-N-triazine (see the insets of Fig. S3). Pre-resonance intensity calculations support that the two bands could be largely enhanced (3.4-fold) with a 633 nm excitation as compared with that of a 532 nm excitation. If compared with off-resonance calculations, the Raman activities in the 392 and 932 cm^{-1} bands show 43.7- and 3.8-fold enhancements, respectively. Theoretically, the expected Raman bands at 334, 350, and 982 cm^{-1}, which are related to the vibrations of the CH_2 of the –N–$(CH_2)_2$–O– and almost independent of Al-O- vibrations, could not be detected.

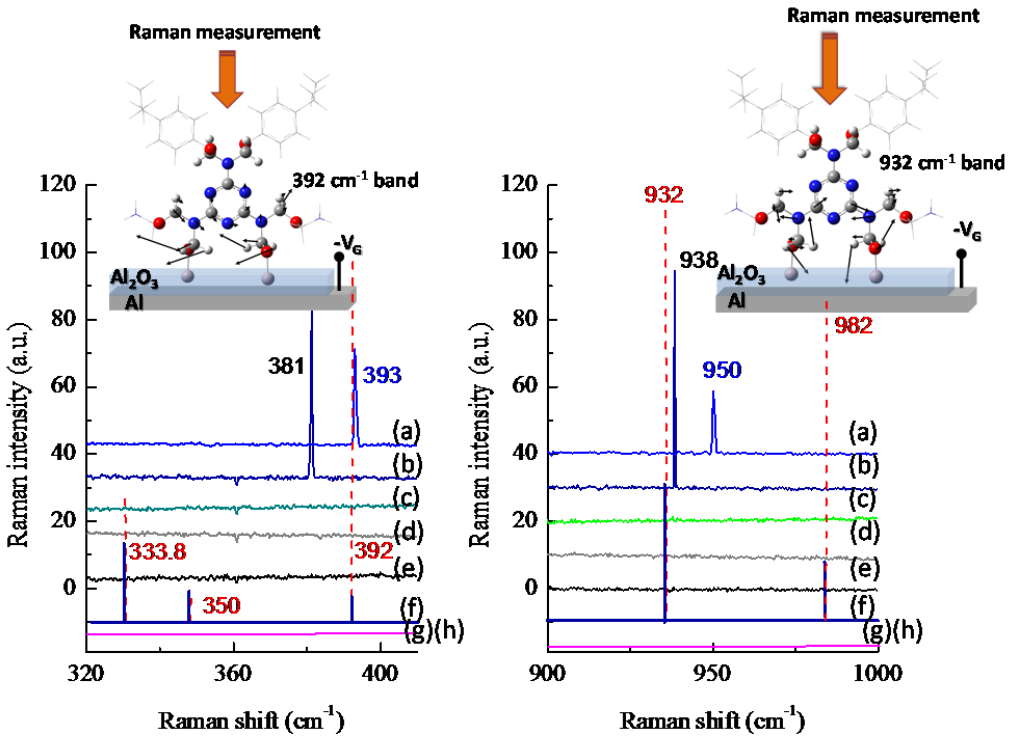

Fig. S3 (a) and (b) are the Raman spectra of the CSDE dielectric sample with an applied V_G of -2.5 V using 532 nm and 633 nm excitation lines (λ_{exc}), respectively. (c) Raman spectrum (λ_{exc} = 633 nm) of the CSDE dielectric sample without an applied voltage. (d) and (e) are the Raman spectra (λ_{exc} = 633 nm) of the Al_2O_3 sample without and with an applied V_G of -2.5 V, respectively. (f), (g), and (h) are the theoretical Raman spectra of the interfacial molecule in the cation, neutral, and anion states, respectively, as determined from the two-layer ONIOM approach (B3LYP/6-31G(d):HF/3-21G*). In the spectral regions from 320 cm^{-1} to 410 cm^{-1} and from 900 cm^{-1} to 1000 cm^{-1}, only the Raman bands with activity exceeding 10^3Å^4/AMU and 10^4Å^4/AMU are shown, respectively. The red dashed line shows the theoretical preresonance intensity with an incident light frequency of 633 nm. The vibrational modes of the 392 cm^{-1} and 932 cm^{-1} bands of the interfacial molecule at the cation state are also shown in the insets, respectively.

Note: Raman spectra of films were recorded using a Jobin Yvon LabRAM HR spectrometer. A 633 nm He−Ne laser and a 532 nm solid-state laser were used as excitation light sources. The spectrometer resolutions for the 633 nm and 532 nm excitation light sources were 0.2 cm^{-1} and 0.4 cm^{-1}, respectively.

4. Microstructural characterization of the pentacene films

Pentacene films grown on the surface of CSDE dielectrics and PMMA/Al_2O_3 dielectrics show common structural features, such as a dominant thin-film phase with a d_{001}-spacing of 15.4 Å, based on XRD measurements (see Fig. S4A). Figs. S3B and S3C show the microRaman spectra and AFM of the pentacene films, respectively. Raman spectroscopy is a powerful tool for characterizing the molecular microstructure and charge-vibrational coupling of organic films in terms of intermolecular vibrational coupling (w) and vibrational reorganization energy (λ).[s2,s3] To ensure efficient charge transport, w must be maximized, whereas λ must be minimized. The w values observed from Davydov splitting of the 1155 cm^{-1} band, which is related to the motion of H-atoms located at the end of the pentacene molecule, are almost the same values (11.9 meV ± 0.1 meV) for both pentacene films. The pentacene films on crosslink-PVP exhibited relatively small full width at half maximum (FWHM) of the Raman bands compared with those of PMMA cases, indicating a small vibrational energy loss during the hole transport processes. Both films exhibited typical grain morphologies. For crosslink-PVP and PMMA, the pentacene films exhibited elongated grain shapes (ca. 2 μm to 3 μm in length) and circular grains (below 1 um in diameter), respectively. The results guarantee a good structural quality of pentacene films on CSDE dielectrics for charge transport.

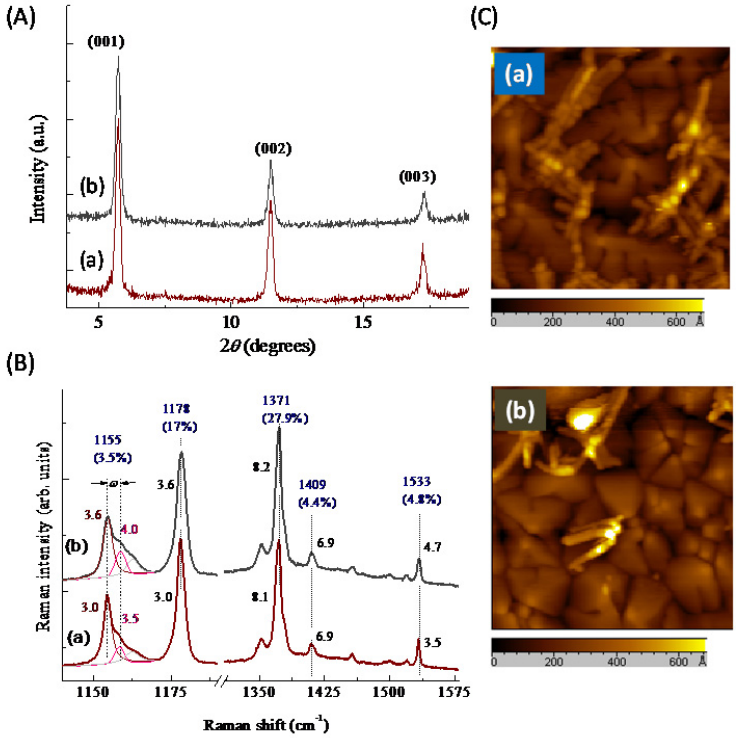

Fig. S4 (A) XRD spectra, (B) microRaman spectra (λ_{exc} = 633 nm), and (C) AFM images (3μm × 3μm) of the pentacene films grown on (a) CSDE dielectric and (b) PMMA/AlO_x surfaces.

Note: XRD spectra of the specimens were produced using a Rigaku RINT 2000 diffractometer with an X-ray wavelength of 1.5406 Å and a scan step size of 0.01°. The surface morphology of pentacene films was measured by AFM (Molecular Imaging Pico Scan 2100).

5. Interfacial trap density (D_{it})

Impedance-admittance analyses[s4] were performed to extract the D_{it} and mean interface trap time constant (τ_{it}); the frequency-dependent conductance at a given V_G was measured. The single time constant model was used, and the equivalent parallel conductance (G_p) is given by

$$\frac{G_P}{\omega} = \frac{q\omega\tau_{it}D_{it}}{1+(\omega\tau_{it})^2} \qquad \text{(s1)}$$

where ω is the angular frequency, q is the charge of the electron, and τ_{it} denotes the mean time constant of the interface state. The maximum value of G_p/ω occurs at $\omega\tau_{it} = 1$. Fig. S5 shows G_p/ω versus frequency. The extracted D_{it} of the CSDE dielectric devices (9.3×10^{11} eV^{-1} cm^{-2}) is twice larger than that of the PMMA/AlO_x devices (4.8×10^{11} eV^{-1} cm^{-2}). However, the τ_{it} value (2.8 μs) is only half of the value of the PMMA/AlO_x devices (τ_{it} = 5.4 μs). The large τ_{it} of the PMMA/AlO_x devices indicate the presence of vacancy-related, long-lifetime charge traps within amorphous PMMA film. Thus, PMMA is shown to be an excellent charge-trapping layer on HfO_2.[44] On the contrary, the crosslink-PVP layer is unsuitable as a charge-trapping layer because of the denser structure resulting from the cross-linking reaction and the lack of large amounts of strong polar functional groups (i.e., –OH).

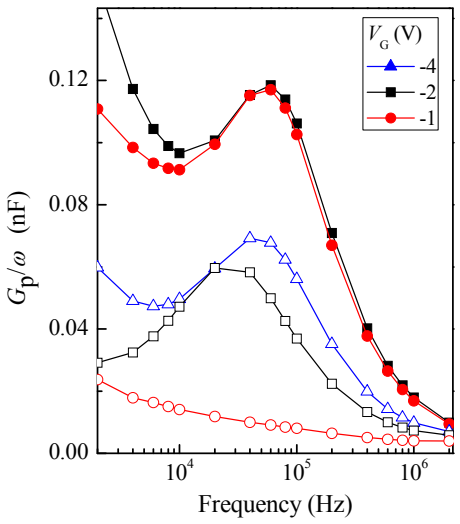

Fig. S5 G_p/ω versus frequency characteristics at selected V_G of the pentacene/CSDE dielectric (closed symbols) and pentacene/PMMA/AlO_x (open symbols) MISM diodes.

6. Supporting electrical characteristics

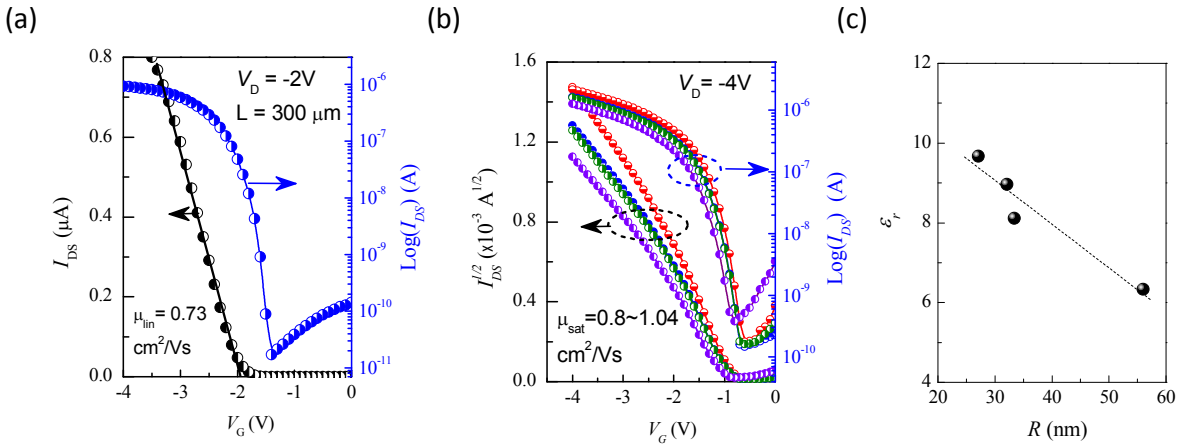

Fig. S6 (a) Linear and (b) saturated transfer curves of pentacene OFETs (with varying channel lengths, L, and constant channel width of 800 μm) using the CSDE dielectrics with thicker crosslink-PVP layer (thickness of ca. 60 nm). Symbols: (red cycles) L=150 μm; (blue cycles) L=200 μm; (Olive cycles) L = 250 μm; (purple cycles) 300 μm. Drain voltage (V_D) and the extracted linear (μ_{lin}) and saturated (μ_{sat}) mobilities are also shown. (c) The dielectric constant (ε_r) varies as a function of thickness of crosslink-PVP layer (R) of the CSDE dielectrics.

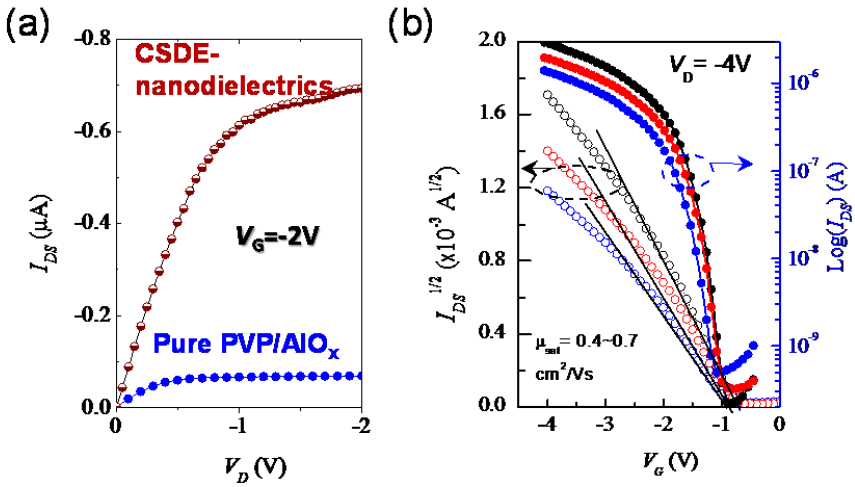

Fig. S7 (a) Output and (b) transfer characteristics of pentacene OFETs (with varying channel lengths, L, and constant channel width of 800 μm) using PVP/AlO$_x$ as gate dielectrics. Symbols: (black cycles) L=100 μm; (red cycles) L=200 μm; (blue cycles) L = 300 μm. Gate voltage (V_G), drain voltage (V_D), and the extracted saturated mobility (μ_{sat}) are also shown. For comparison, output curve of pentacene OFETs with CSDE dielectrics (wine cycles, L=300 μm) are shown in (a).

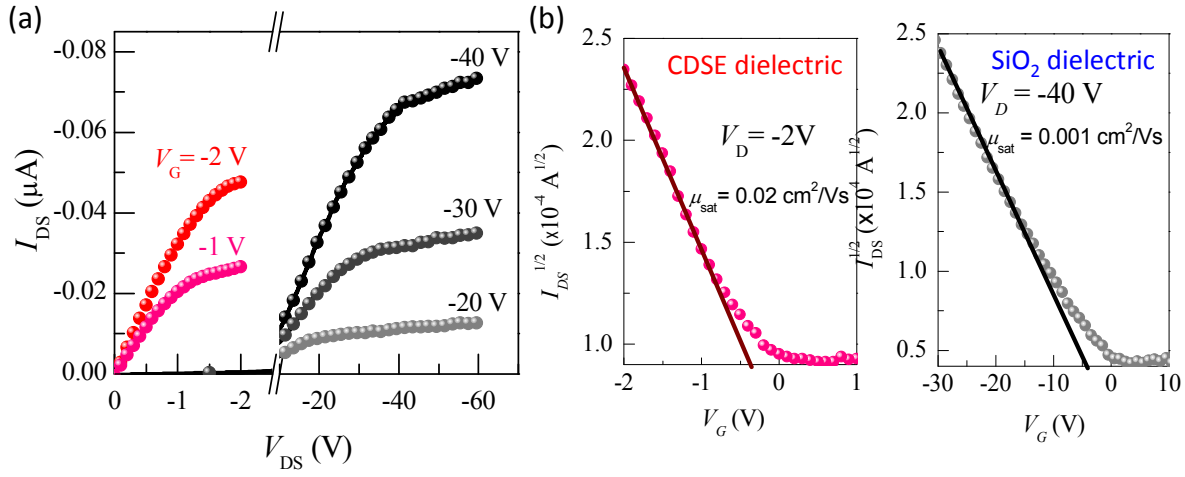

Fig. S8 Comparison of (a) output and (b) transfer characteristics of P3HT-based FETs using SiO_2 (black symbols, obtained in nitrogen atmosphere) and CSDE (red symbols, obtained in air atmosphere) dielectrics as gate dielectrics. Gate voltage (V_G), drain voltage (V_D), and the extracted saturated mobility (μ_{sat}) are also shown.

References

s1 K. Shimizu, C. Phanopoulos, R. Loenders, M.-L. Abela and J. F. Wattsa, *Surf. Interface Anal.,* 2010, **42**, 1432.

s2 H. L. Cheng, Y. S. Mai, W. Y. Chou, L. R. Chang and X. W. Liang, *Adv. Funct. Mater.,* 2007, **17**, 3639.

s3 H. L. Cheng, X. W. Liang, W. Y. Chou, Y. S. Mai, C. Y. Yang, L. R. Chang and F. C. Tang, *Org. Electron.,* 2009, **10**, 289.

s4 E. H. Nicollian and J. R. Brews, *MOS Physics and Technology.* Wiley, New York, 1981.